Delta-Doping for Enhanced III-V Tunnel Junction Performance

Yukun Sun, Shizhao Fan, Daehwan Jung, Ryan D Hool, Brian Li, Michelle Vaisman, and Minjoo Lee, *Senior Member, IEEE*

***Abstract*—We show that delta-doping boosts the performance of tunnel junctions (TJs) used as interconnects in III-V multijunction solar cells by orders of magnitude. The peak current of our baseline TJ design consisting of p-GaAs/n-GaAs surrounded by $Ga_{0.51}In_{0.49}P$ clads is improved by a factor of $\sim 5 \times 10^5$. The relative benefits of delta-doping are even stronger in TJs based on wider-bandgap materials with reduced optical absorption. Importantly, we find that delta-doped TJs can survive the thermal loads that would be encountered during growth of additional subcells. Delta doping is a simple and versatile method to improve TJ performance that can be implemented by virtually any epitaxial growth method.**

***Index Terms*—Delta doping, tunnel junctions (TJs).**

I. Introduction

TUNNEL junctions (TJs) in III-V multijunction solar cells (MJSCs) should be transparent or nearly transparent to light intended for lower subcells in order to prevent parasitic absorption, favoring the use of materials with wide bandgap energies (E_g). However, both the tunneling probability [1], [2] and the ability to achieve degenerate doping of both types [3] improve as E_g narrows. Considering the heavy doping levels involved, a further challenge for TJs is thermal degradation during growth of additional sub-cells. Both metalorganic vapor phase epitaxy (MOVPE) and hydride vapor phase epitaxy (HVPE) are carried out at growth temperatures T $\sim$ 600 °C for several minutes to several hours. Out-diffusion of dopants from heavily doped TJ layers can be significant, resulting in greatly decreased tunneling [4]. Additionally, postgrowth rapid thermal annealing (RTA) at T = 650–800 °C has been shown to improve the performance of both dilute nitride [5] and phosphide [6], [7] materials grown by molecular beam epitaxy (MBE), placing further demands on TJs.

The main performance figures of merit for TJs used in MJSCs are specific resistance ($R_{\rm spec}$) near the origin, which should be minimized, and peak current density ($J_{\rm peak}$), which must exceed the current density at maximum power ($J_{\rm mp}$); for one-sun operation, $J_{\rm mp}$ for an MJSC may be $\sim$10 mA/cm^2, whereas for high-concentration photovoltaics $J_{\rm mp}$ can be on the order of $\sim$1–30 A/cm^2. Even with high radiative and quantum efficiency in the individual sub-cells, a single low-performance TJ can greatly hamper the efficiency of an MJSC [8], [9].

The challenges and contradictory requirements for TJs used in MJSCs have prompted researchers to develop wide-ranging methods to improve their performance. Boosting trap-assisted tunneling, as opposed to band-to-band tunneling (BTBT), can enable low $R_{\rm spec}$, and such TJs were reported earlier with As precipitates [10], [11] and ErAs nanoparticles to provide trap states [12]–[14] [15]. However, Er is not commonly used in commercial III-V growth systems. For stronger BTBT, design features such as quantum wells [2], [16], [17] and wide-E_g clads [4], [18], [19] have been widely reported, and both are incorporated in the TJs described here. Delta-doping (δ-doping) is another promising technique to improve TJ performance that is compatible with most III-V growth methods. A δ-doping spike is generated by simply pausing the flux of group-III sources while maintaining the flux of the dopant and group-V sources. The growth pauses significantly increase local doping levels [20], while the group-V overpressure suppresses the amphotericity of group-IV dopants, such as Si; Si δ-doping was earlier used to reduce contact resistances to n-GaAs [20] where the thermodynamically stable electron concentration is limited to

Manuscript received March 11, 2022; accepted March 24, 2022. Date of publication June 1, 2022; date of current version June 21, 2022. This work was supported by the ARPA-E FOCUS program under Award DE-AR0000508. The work of Ryan D Hool and Brian Li was supported by National Aeronautics and Space Administration Space Technology Research Fellowships under Grant 80NSSC18K1171 and Grant 80NSSC19K1174, respectively. *(Corresponding author: Minjoo Lee.)*

Yukun Sun was with the Department of Electrical Engineering, Yale University, New Haven, CT 06520 USA. He is now with the Department of Electrical and Computer Engineering, University of Illinois at Urbana-Champaign, Urbana, IL 61801 USA, and also with the Nick Holonyak, Jr. Micro and Nanotechnology Laboratory, Urbana, IL 61801 USA (e-mail: ys446@illinois.edu).

Shizhao Fan was with the Department of Electrical and Computer Engineering, University of Illinois at Urbana-Champaign, Urbana, IL 61801 USA, and also with the Nick Holonyak, Jr. Micro and Nanotechnology Laboratory, Urbana, IL 61801 USA. He is now with the Suzhou Institute of Nano-Tech and Nano-Bionics, Suzhou 215123, China (e-mail: szfan2020@sinano.ac.cn).

Daehwan Jung was with the Department of Electrical Engineering, Yale University, New Haven, CT 06520 USA. He is now with the Center for Optoelectronic Materials and Devices and University of Science and Technology, Korea Institute of Science and Technology, Seoul 02792, South Korea (e-mail: daehwan.jung@kist.re.kr).

Ryan D Hool is with the Department of Materials Science and Engineering, University of Illinois at Urbana-Champaign, Urbana, IL 61801 USA, and also with the Nick Holonyak, Jr. Micro and Nanotechnology Laboratory, Urbana, IL 61801 USA (e-mail: rhool2@illinois.edu).

Brian Li and Minjoo Lee are with the Department of Electrical and Computer Engineering, University of Illinois at Urbana-Champaign, Urbana, IL 61801 USA, and also with the Nick Holonyak, Jr. Micro and Nanotechnology Laboratory, Urbana, IL 61801 USA (e-mail: bdli2@illinois.edu; mllee@illinois.edu).

Michelle Vaisman was with the Department of Electrical Engineering, Yale University, New Haven, CT 06520 USA. She is now with the Bain and Company, Boston, MA 02116 USA (e-mail: vaisman.m.a@gmail.com).

Color versions of one or more figures in this article are available at https://doi.org/10.1109/JPHOTOV.2022.3176217.

Digital Object Identifier 10.1109/JPHOTOV.2022.3176217

$\sim$5–6 $\times$ 10^{18} cm^{-3} [21]. The high n-type doping levels close to a δ-doping spike promote BTBT by strongly bending the bands and pushing the Fermi level into the conduction band [1], [22]. δ-doped GaAs TJs were previously reported by DeSalvo [23] and Ragay [24] though the performance was moderate. More recently, Kang *et al.* [22] reported δ-doped GaAs TJs with high $J_{\rm peak}$ up to 2.74 kA/cm^2, though their designs suffer from significant optical losses due to the use of a thick 30 nm GaAs tunnel region. Moreover, the bulk Si doping level on the *n*-type side of Kang's δ-doped GaAs TJs was 1 $\times$ 10^{19} cm^{-3}, making them unstable against thermal loading above $\sim$600 °C [25]. Neither the effectiveness of δ-doping for enhancement of TJs with low optical absorption nor their operation after thermal loading required for top cell growth have been established in the literature to data; both are required for δ-doped TJs to be used in MJSCs.

In this article, we demonstrate that $J_{\rm peak}$ ($R_{\rm spec}$) of GaAs-based TJ designs employing thin tunneling regions and wide-E_g clads can be increased (decreased) by orders of magnitude via δ-doping. We also describe TJs with high optical transparency that fail to exhibit any Esaki peak without δ-doping while tunneling strongly with δ-doping. δ-doped TJs are also shown for the first time to be robust to typical thermal loads that would be encountered in MBE, MOVPE, and HVPE.

Compared to our previous conference proceedings [26], this article provides more growth details, additional materials characterization, calculations of optical transparency, and new experiments to determine how δ-doped TJs function after thermal loading. In particular, we use cross-sectional transmission electron microscopy (XTEM) to show the absence of extended defects such as dislocations or stacking faults in δ-doped TJs. We also provide calculations of parasitic optical absorption in all of the investigated TJ designs, allowing the reader to gain greater understanding of how MJSC current matching might be affected. Finally, while our conference proceeding showed that δ-doped TJs function after thermal loading from both MBE growth and postgrowth RTA at 800 °C, we performed additional anneals here at 600 °C and 700 °C to ascertain the potential performance of δ-doped TJs in MOVPE and HVPE growth conditions.

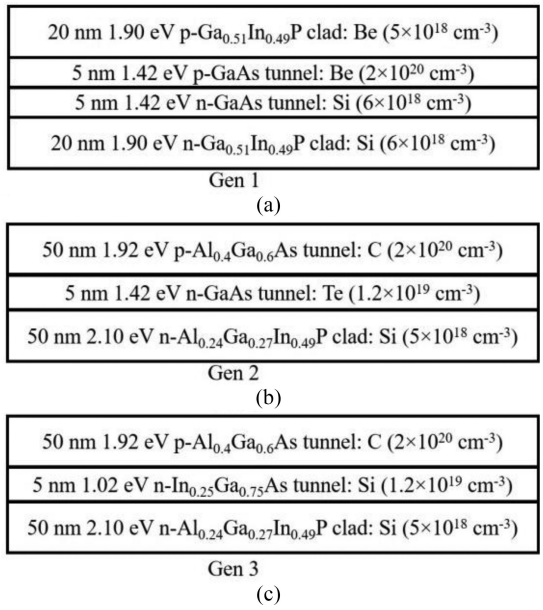

Fig. 1. Schematic layer structures of (a) Gen 1, (b) Gen 2, and (c) Gen 3 TJs studied in this article.

TABLE I
GROWTH CONDITIONS USED IN TJS STUDIED IN THIS ARTICLE

Layer	Background doping (cm^{-3})	Growth rate (μm/h)	V/III ratio
1.90 eV p-GaInP clad	Be, 5×10^{18}	0.2	40
1.42 eV p-GaAs tunnel	Be, 2×10^{20}	0.1	30
1.42 eV n-GaAs tunnel + varying δ-spikes	Si, 6×10^{18}	0.1	150
1.90 eV n-GaInP clad	Si, 6×10^{18}	0.2	100
1.92 eV p-AlGaAs tunnel	C, 9×10^{19} or 2×10^{20}	0.24	75
1.42 eV n-GaAs tunnel + 3× δ-spikes	Te, 1.2×10^{19}	0.1	150
2.10 eV n-AlGaInP clad	Si, 5×10^{18}	0.17	150
1.02 eV n-InGaAs tunnel + 3× δ-spikes	Si, 1.2×10^{19}	0.37	50

II. EXPERIMENTS

Several design variations (Gen 1 to Gen 3, Fig. 1) were implemented to investigate the tradeoffs between tunneling performance, thermal degradation, and optical transparency. In Gen 1 TJs, the effectiveness of Si δ-doping was demonstrated using GaAs tunneling layers, yielding the best performance and the lowest optical transparency; further details on estimated optical losses are given below. Gen 2 TJs focused on suppressing parasitic absorption by switching to wider-E_g materials, and as a result, the best optical transparency was accomplished at the cost of stronger thermal degradation. Finally, Gen 3 TJs were designed to balance the respective advantages of the Gen 1 and 2 designs.

All TJ samples were grown via solid-source MBE at 460 °C (as measured by pyrometry), similar to the phosphide growth temperature used in our previous work [6], [7], and carrier concentrations were estimated from Hall effect measurements of separate calibration samples; details of growth conditions are given in Table I. δ-doping was accomplished by closing all group-III shutters for a pre-determined time (typically several minutes) while maintaining the molecular beam flux of both the *n*-type dopant and group V species. The δ-doping dosages are given in this article in terms of fraction of a monolayer (ML), where the atomic density of the GaAs (001) surface is 6.26 $\times$ 10^{14} cm^{-2}; 0.01 ML therefore refers to a nominal surface dopant atom concentration of 6.26 $\times$ 10^{12} cm^{-2}. The deposition time for the designed dosage was calculated based on dopant atomic flux (cm$^{-2}\cdot$s^{-1}) from bulk doping calibrations. For Gen 1 TJs, a single δ-spike consisting of 0.01–0.08 ML coverage of Si was inserted in the middle of the 5 nm n-GaAs tunnel layer [see Fig. 1(a)]. Another Gen 1 TJ was grown with 2 $\times$ 0.04 ML δ-spikes at 1.6 and 3.3 nm of the 5 nm n-GaAs layer to study

the effects of δ-doping geometry on TJ performance. For Gen 2 [see Fig. 1(b)] and Gen 3 [see Fig. 1(c)] TJs, the following changes were made: the *p*-type doping was switched from 2×10^{20} cm^{-3} by Be to 9×10^{19} cm^{-3} by C; the GaInP clads were replaced with p-$Al_{0.4}Ga_{0.6}As$ ($E_g = 1.92$ eV, hereafter AlGaAs), and n-$Al_{0.17}Ga_{0.35}In_{0.48}P$ ($E_g = 2.10$ eV, hereafter AlGaInP), to facilitate C-doping [27] and improve optical transparency, respectively; the 5 nm p-GaAs layer was eliminated to improve optical transparency. In the Gen 2 design, the *n*-type dopant was switched to Te, and 3×0.04 ML δ-spikes of Te were inserted at 0.5, 2.5, and 4.5 nm of the 5 nm n-GaAs layer. Another version of the Gen 2 and 3 TJs was also grown with C-doping boosted from 9×10^{19} to 2×10^{20} cm^{-3} in the p-AlGaAs. In the Gen 3 design, the n-GaAs layer was replaced with n-$In_{0.25}Ga_{0.75}As$ ($E_{g,\ \mathrm{bulk}} = 1.02$ eV, hereafter InGaAs) as a means to improve BTBT probability due to its lower E_g and stronger propensity for n-type doping [3], [28] at the cost of increased optical absorption; the InGaAs layer was kept below the critical thickness of ~6 nm.

XTEM samples were prepared by manual thinning followed by Ar ion milling. Bright-field imaging was carried out in a JEOL 2010 microscope operated at 200 kV with a LaB_6 filament using a $g = <002>$ two-beam condition.

Pieces were cleaved from as-grown samples, coated with SiO_2 by plasma-enhanced chemical vapor deposition to prevent excessive anion desorption, and annealed in a tube furnace at 480 °C for 3 h to replicate MBE growth conditions for (Al) GaInP top cells [6], [29]. After the 480 °C tube furnace annealing, some pieces underwent additional RTA at 800 °C for 30 s in N_2 ambient, which improves MBE-grown phosphide top cell performance [7]. Furnace annealing experiments at 600 °C and 700 °C for 3 hours were also performed on separate pieces to study stability under thermal loads that might be encountered in MOVPE and HVPE (while the growth temperature in HVPE is similar to MOVPE, growth times can be significantly lower [30]–[33]). As-grown and annealed samples were fabricated into TJs with areas of 9×10^{-5}–1×10^{-3} cm^2 using standard photolithography, lift-off, and wet-etching techniques. Four-wire measurements were found necessary to obtain reproducible current density-voltage (*JV*) characteristics of TJs, and a MATLAB program was used to extract TJ parameters.

III. Results

A. Materials Characterization

Fig. 2 shows that moderate Si δ-doping neither roughens the growth surface nor creates high densities of extended defects. The n-GaAs tunneling layer presents a streaky reflection high-energy electron diffraction (RHEED) pattern [see Fig. 2(a)], indicative of planar growth. The RHEED pattern remained streaky during [see Fig. 2(b)] and after the deposition of δ-spikes when the dosage was kept no greater than 0.08 ML, indicating minimal surface roughening; a separate experiment showed a spotty RHEED pattern when the dosage was increased to 0.16 ML, so an upper limit of δ-doping dosage likely exists. XTEM did not reveal any dislocations or stacking faults initiated at the δ-doping interface [see Fig. 2(c)]. TJs with δ-doping have no effect on the growth surface morphology and, within the limits of XTEM, do not contribute to significant formation of extended defects, making them promising for use in MJSCs.

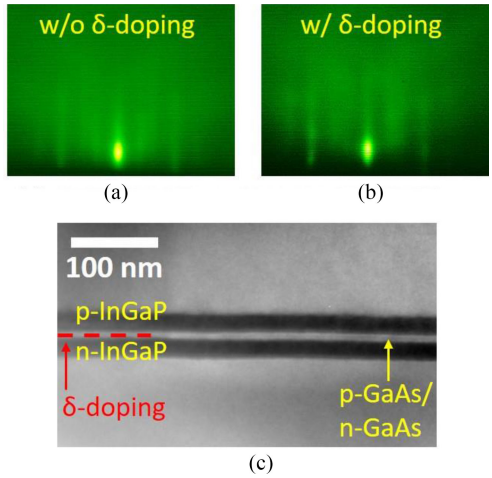

Fig. 2. RHEED pattern (a) during the growth of n-GaAs tunnel layer of Gen 1 control TJ. (b) At the end of 0.04 ML δ-doping deposition in Gen 1 TJs, where streaky patterns indicate minimal surface roughness. (c) Bright-field XTEM image (g=<002>) of Gen 1 TJ with 0.08 ML δ-doping, showing no dislocations or stacking faults in the TJs.

TABLE II
Gen 1 TJ Performance Before Annealing

Sample	J_{peak} (A/cm^2)	R_{spec} (Ω·cm^2)
2×0.04 ML	3.59×10^{3}	1.32×10^{-4}
0.08 ML	1.87×10^{3}	2.06×10^{-4}
0.02 ML	2.51×10^{1}	5.48×10^{-3}
0.01 ML	1.42×10^{-1}	3.39×10^{-1}
Control	7.32×10^{-3}	4.98×10^{0}

B. TJ Performance Enhancement by δ-Doping

δ-doping singlehandedly transforms the Gen 1 TJ from a low- to a high-performance device, as evident by the orders of magnitude improvements in its key figures of merit. Control Gen 1 TJs without δ-doping [see Fig. 3(a), red] are incapable of flowing sufficient current to permit 1-sun operation (see Table II). With the addition of just 0.01 ML of Si δ-doping [see Fig. 3(a), yellow] the TJ performance is adequate for 1-sun operation, while a TJ with 2×0.04 ML δ-doping spikes attained $J_{\mathrm{peak}} = 3.59 \times 10^3$ A/cm^2. Although the total dosage of δ-doping remains the same for both 0.08 and 2×0.04 ML designs and our band simulation shows only minor differences in tunneling distance between the two, the 2×0.04 ML design shows stronger TJ performance, possibly from reduced amphoteric compensation. Future study on the effects of δ-doping dose and location on TJ performance could help elucidate reasons for the observed behavior. R_{spec} decreased with increasing J_{peak} (see Table II) and the lowest R_{spec} value in this article was 1.32×10^{-4} Ωcm^2 for the 2×0.04 ML δ-doped TJ, which is slightly lower than

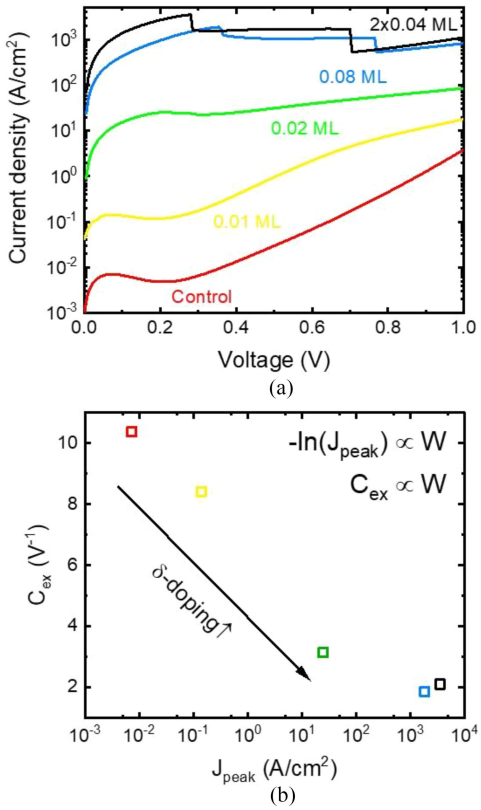

Fig. 3. (a) *JV* characteristics of Gen 1 TJs with δ-doping. (b) Correlation between $C_{\rm ex}$ and $J_{\rm peak}$ as Gen 1 TJ performance improves supporting BTBT as the tunneling mechanism. Figure adopted from [26].

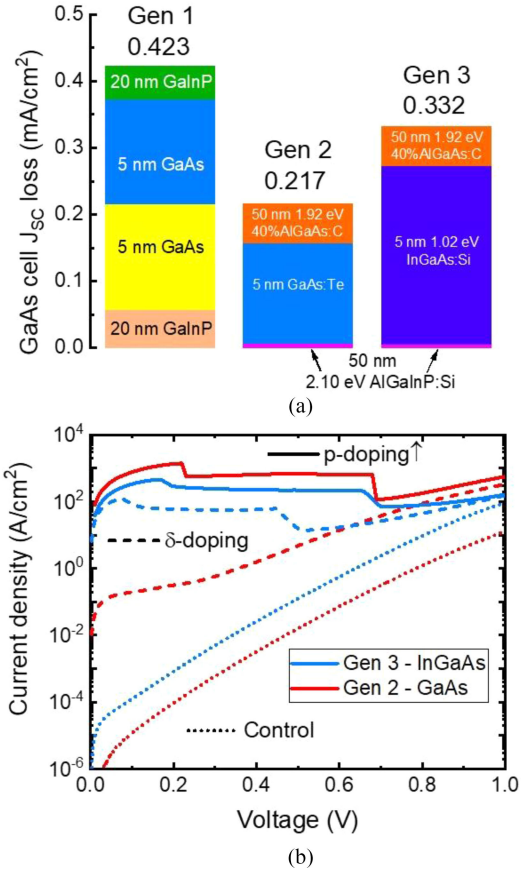

Fig. 4. (a) Calculated GaAs cell $J_{\rm SC}$ loss (based on AM1.5G spectrum) under 800 nm GaInP top cell in Gen 1–3 TJs, emphasizing the benefit of wide-E_g materials for optical transparency. (b) Evolution of Gen 2 and 3 *JV* characteristics by adding 3 $\times$ 0.04 ML δ-doping (dashed) and further increasing *p*-type doping in AlGaAs (solid) from control (dotted).

the value reported by Kang *et al.* [22]. The decreasing value of the excess current parameter $C_{\rm ex}$ with increasing $J_{\rm peak}$ [see Fig. 3(b)], further emphasizes that increased BTBT is the main mechanism for improved performance [1], [22], [34]. We determine $C_{\rm ex}$, a unitless from of depletion width, [1], [34] based on *JV* data using the empirical expression $J = J_{\rm ex}\exp(C_{\rm ex}\cdot V)$. Using a Poisson's equation solver, we found a depletion width reduction of $\sim$5 $\times$, from 16.7 nm in the control device to 2.92 nm in the 2 $\times$ 0.04 ML TJ. The reduction of $C_{\rm ex}$ with increasing $J_{\rm peak}$ points to a reduction in depletion width with δ-doping and indicates that increased BTBT, as opposed to increased trap-assisted tunneling, is the primary mechanism for enhanced TJ performance where depletion width is not changed.

C. TJs With Improved Optical Transparency

Through the use of wider-E_g materials and the reduction of GaAs thickness, Gen 2 and 3 TJs reduced the parasitic absorption compared to Gen 1 by up to 48%. Assuming a 1.88 eV GaInP top cell (800 nm), we estimated the parasitic $J_{\rm SC}$ loss due to each layer of the Gen 1–3 TJs in an underlying GaAs cell [see Fig. 4(a), based on AM1.5G spectrum]. Absorption in the GaInP top cell and TJ layers was estimated based on layer thickness and optical indices of GaInP, AlGaInP, GaAs, and AlGaAs. Bottom cell $J_{\rm SC}$ was calculated from the remaining spectrum using the internal quantum efficiency of a high-performance GaAs cell from our lab. $J_{\rm SC}$ loss of 0.423 mA/cm^2 in Gen 1 is reduced to 0.217 mA/cm^2 in Gen 2 by substituting n-GaInP with 2.10 eV n-AlGaInP and eliminating the 5 nm p-GaAs layer. Meanwhile, Gen 3 exhibited reduced thermal degradation with the lower-E_g *n*-type InGaAs layer (as shown later), at the cost of optical transparency, causing 0.332 mA/cm^2 $J_{\rm SC}$ loss in the GaAs bottom cell. The same assumptions yielded 0.156–2.62 mA/cm^2 of GaAs cell $J_{\rm SC}$ loss for previously reported state-of-the-art TJs [16], [18], [35], comparable to or worse than the Gen 1–3 TJs described here.

δ-doping, together with heavy *p*-type doping, was essential to attain strong tunneling in Gen 2 and 3 TJs, as BTBT probability exponentially decreases with increasing E_g [1]. Gen 2 and 3 TJs without δ-doping [dotted lines in Fig. 4(b)] fail to tunnel at all. With the addition of 3 $\times$ 0.04 ML n-type δ-doping spikes, $J_{\rm peak}$ values of 0.269 and 116 A/cm^2 were obtained in Gen 2 and Gen 3 TJs, respectively [dashed lines in Fig. 4(b)]. We attribute the improved tunneling characteristics of the Gen 3 device over Gen 2 to its use of the narrower-E_g n-InGaAs layer. Boosting the *p*-type doping of the AlGaAs to 2 $\times$ 10^{20} cm^{-3} further enhanced performance to $J_{\rm peak} = 1346$ and 440 A/cm^2 and $R_{\rm spec} = 1.23 \times 10^{-4}$ and 2.67 $\times$ 10^{-4} Ωcm^2 in Gen 2 and 3 TJs, respectively [solid lines in Fig. 4(b)].

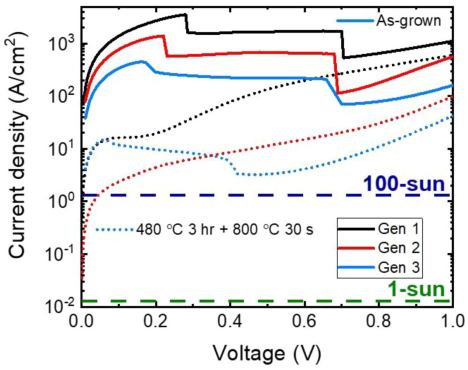

Fig. 5. *JV* characteristics of Gen 1–3 TJs as-grown (solid) and after 480 °C 3 h and 800 °C 30 s annealing (dotted), with dashed lines marking the approximate operating current of MJSCs under 100 × (navy) and 1 × (green).

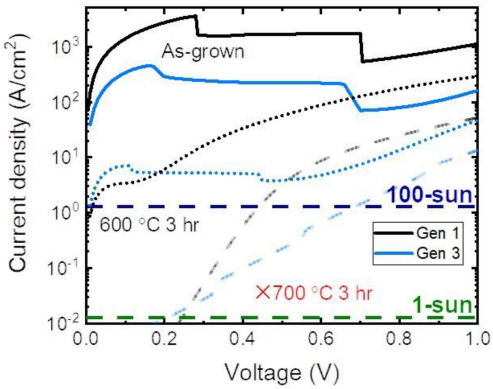

Fig. 6. *JV* characteristics of Gen 1 and 3 TJs as-grown (solid) and after 600 °C 3 h (dotted) and 700 °C 3 h (dashed).

TABLE III
GEN 1–3 TJ PERFORMANCE BEFORE AND AFTER 480 °C 3 H AND 800 °C 30 S THERMAL TREATMENT

Sample		J_{peak} (A/cm^2)	R_{spec} (Ω·cm^2)
As-grown	Gen 1	3.59×10^{3}	1.32×10^{-4}
	Gen 2	1.34×10^{3}	1.23×10^{-4}
	Gen 3	4.40×10^{2}	2.67×10^{-4}
480 °C 3 h	Gen 1	2.71×10^{2}	5.43×10^{-4}
	Gen 2	1.16×10^{3}	1.44×10^{-4}
	Gen 3	1.80×10^{2}	1.20×10^{-3}
480 °C 3 h + 800 °C 30 s	Gen 1	1.52×10^{1}	2.49×10^{-3}
	Gen 2	4.72×10^{0}	2.75×10^{-2}
	Gen 3	1.50×10^{1}	3.19×10^{-3}

TABLE IV
GEN 1 AND 3 TJ PERFORMANCE BEFORE AND AFTER 600 °C 3 H THERMAL TREATMENT

Sample		J_{peak} (A/cm^2)	R_{spec} (Ω·cm^2)
As-grown	Gen 1	3.59×10^{3}	1.32×10^{-4}
	Gen 3	4.40×10^{2}	2.67×10^{-4}
600 °C 3 h	Gen 1	3.08×10^{0}	1.60×10^{-2}
	Gen 3	6.95×10^{0}	8.66×10^{-3}

D. Thermal Degradation of TJs

Although a decrease (increase) in J_{peak} (R_{spec}) occurred after annealing (see Fig. 5 and Table III), the performance of δ-doped TJs remains sufficient for >100 × concentration. Slight performance loss was observed in Gen 1–3 TJs after undergoing MBE (Al)GaInP top cell growth thermal load of 3 h at 480 °C; Gen 2 showed minimal J_{peak} and R_{spec} change while Gen 1 exhibited ∼10 × J_{peak} decrease (see Table III). Despite its short annealing time, RTA at 800 °C caused large performance degradation in all TJs (see Fig. 5 and Table III), suggesting that thermally activated processes (e.g., dopant diffusion and/or deactivation) contribute to performance change [16], [25], [36]. J_{peak} (R_{spec}) of Gen 1 TJs dropped (increased) from 3.59×10^3 A/cm^2 (1.32×10^{-4} Ωcm^2) to 15.2 A/cm^2 (2.49×10^{-3} Ωcm^2) after 480 °C 3 h and 800 °C 30 s, but can nevertheless support MJSC operation at ∼100 × concentration with negligible series resistance losses. The Gen 2 TJ's performance loss was particularly strong (two orders of magnitude J_{peak} decrease and R_{spec} increase from as-grown devices), possibly due to its use of relatively wider-E_g tunneling layers (p-AlGaAs/n-GaAs) compared to Gen 1 (p-GaAs/n-GaAs) and Gen 3 (p-AlGaAs/n-InGaAs); Gen 2 TJs were not included in further thermal degradation experiments. As mentioned earlier, the use of narrower-E_g InGaAs in Gen 3 reduced its thermal degradation, providing 15.0 A/cm^2 J_{peak} and 3.19 × 10^{-3} Ωcm^2 R_{spec}, similar to Gen 1 after RTA (see Fig. 5).

The Gen 1 and 3 TJs perform well after holding at 600 °C for 3 h, indicating that the benefits of δ-doping may also be robust to MOVPE/HVPE growth conditions. Strong BTBT peaks (3.08 and 6.95 A/cm^2) together with R_{spec} of 1.60×10^{-2} and 8.66×10^{-3} Ωcm^2 in Gen 1 and 3, respectively, support MJSC operation up to 5–10 × concentration with <1 mV voltage drop (see Fig. 6 and Table IV); the high-performance enabled by δ-doping provides a large degree of headroom for thermal degradation. The better performance and smaller degradation after 600 °C thermal treatment in Gen 3 (blue) compared to Gen 1 (black) in Fig. 6 reinforces the importance of the narrower-E_g n-InGaAs tunnel Layer. Neither TJ survived 700 °C annealing for 3 h (dashed lines in Fig. 6), and based on our findings, we speculate that the use of C doping in the Gen 1 design could potentially enable greater stability.

IV. CONCLUSION

In this article, we showed that δ-doping provides significant benefits for TJs due to its strong band-bending over short distances. The use of wide-E_g materials, such as AlGaAs and AlGaInP in Gen 2 and 3 designs enhanced optical transparency and

underscored the importance of δ-doping for high performance. While the δ-doped TJs investigated here were grown by MBE, the performance after 3 h at 600 °C indicates that the benefits of δ-doping likely extend to both MOVPE and HVPE. Reduced thermal degradation was obtained in the Gen 3 design by substituting the GaAs tunneling layer with narrower-E_g InGaAs at the cost of an increase in parasitic absorption. Further reductions in the thickness of the GaAs or InGaAs layers could lead to device designs with lower optical losses.

ACKNOWLEDGMENT

The research was carried out in part at the Frederick Seitz Materials Research Laboratory Central Facilities, University of Illinois at Urbana-Champaign.

REFERENCES

[1] S. M. Sze and K. K. Ng, *Physics of Semiconductor Devices*. Hoboken, NJ, USA: Wiley, 2006.

[2] M. Vaisman, K. N. Yaung, Y. Sun, and M. L. Lee, "GaAsP/Si solar cells and tunnel junctions for III-V/Si tandem devices," in *Proc. IEEE 43rd Photovolt. Specialists Conf.*, 2016, pp. 2043–2047, doi: 10.1109/PVSC.2016.7749988.

[3] W. Walukiewicz, "Intrinsic limitations to the doping of wide-gap semiconductors," *Phys. B Condens. Matter*, vol. 302–303, pp. 123–134, 2001.

[4] P. Colter, B. Hagar, and S. Bedair, "Tunnel junctions for III-V multijunction solar cells review," *Crystals*, vol. 8, no. 12, p. 445, 2018.

[5] D. B. Jackrel *et al.*, "Dilute nitride Gainnas and Gainnassb solar cells by molecular beam epitaxy," *J. Appl. Phys.*, vol. 101, no. 11, 2007, Art. no. 114916, doi: 10.1063/1.2744490.

[6] J. Faucher *et al.*, "High-efficiency AlGaInP solar cells grown by molecular beam epitaxy," *Appl. Phys. Lett.*, vol. 109, no. 17, 2016, Art. no. 172105, doi: 10.1063/1.4965979.

[7] Y. Sun *et al.*, "2.0–2.2 eV AlGaInP solar cells grown by molecular beam epitaxy," *Sol. Energy Mater. Sol. Cells*, vol. 219, 2021, Art. no. 110774.

[8] A. W. Walker, O. Thériault, M. M. Wilkins, J. F. Wheeldon, and K. Hinzer, "Tunnel-Junction-Limited multijunction solar cell performance over concentration," *IEEE J. Sel. Top. Quantum Electron.*, vol. 19, no. 5, Sep./Oct. 2013, Art. no. 4000508, doi: 10.1109/JSTQE.2013.2258140.

[9] J. F. Geisz *et al.*, "Six-junction III–V solar cells with 47.1% conversion efficiency under 143 suns concentration," *Nature Energy*, vol. 5, pp. 326–335, 2020.

[10] S. Ahmed, M. R. Melloch, E. S. Harmon, D. T. McInturff, and J. M. Woodall, "Use of nonstoichiometry to form GaAs tunnel junctions," *Appl. Phys. Lett.*, vol. 71, no. 25, pp. 3667–3669, 1997.

[11] S. Ahmed, M. R. Melloch, D. T. McInturff, J. M. Woodall, and E. S. Harmon, "Low-temperature grown GaAs tunnel junctions," *Electron. Lett.*, vol. 33, no. 18, pp. 1585–1587, 1997.

[12] J. M. O. Zide *et al.*, "Increased efficiency in multijunction solar cells through the incorporation of semimetallic ErAs nanoparticles into the tunnel junction," *Appl. Phys. Lett.*, vol. 88, no. 16, 2006, Art. no. 162103.

[13] P. Pohl *et al.*, "Enhanced recombination tunneling in GaAs pn junctions containing low-temperature-grown-GaAs and ErAs layers," *Appl. Phys. Lett.*, vol. 83, no. 19, pp. 4035–4037, 2003.

[14] H. P. Nair, A. M. Crook, and S. R. Bank, "Enhanced conductivity of tunnel junctions employing semimetallic nanoparticles through variation in growth temperature and deposition," *Appl. Phys. Lett.*, vol. 96, no. 22, 2010, Art. no. 222104.

[15] A. M. Crook *et al.*, "Annealing stability of nanoparticle-enhanced tunnel junctions for high-efficiency solar cells and mid-infrared lasers," in *Proc. 51st Electron. Mater. Conf.*, 2009.

[16] S. M. Bedair, J. L. Harmon, C. Z. Carlin, I. E. H. Sayed, and P. C. Colter, "High performance as-grown and annealed high band gap tunnel junctions: Te behavior at the interface," *Appl. Phys. Lett.*, vol. 108, no. 20, 2016, Art. no. 203903.

[17] M. P. Lumb *et al.*, "High temperature current-voltage characteristics of InP-based tunnel junctions: Temperature dependent characteristics of tunnel-junctions," *Prog. Photovolt. Res. Appl.*, vol. 23, no. 6, pp. 773–782, 2015.

[18] D. J. Chmielewski *et al.*, "High performance metamorphic tunnel junctions for GaAsP/Si tandem solar cells grown via MOCVD," in *Proc. IEEE 7th World Conf. Photovolt. Energy Convers., Joint Conf. 45th IEEE PVSC, 28th PVSEC 34th EU PVSEC*, 2018, pp. 2631–2634, doi: 10.1109/PVSC.2018.8547444.

[19] I. García, I. Rey-Stolle, and C. Algora, "Performance analysis of AlGaAs/GaAs tunnel junctions for ultra-high concentration photovoltaics," *J. Phys. Appl. Phys.*, vol. 45, no. 4, 2012, Art. no. 045101.

[20] E. F. Schubert, "Delta doping of III–V compound semiconductors: Fundamentals and device applications," *J. Vaccum Sci. Technol. A*, vol. 8, no. 3, pp. 2980–2996, May 1990.

[21] Y. G. Chai, R. Chow, and C. E. C. Wood, "The effect of growth conditions on Si incorporation in molecular beam epitaxial GaAs," *Appl. Phys. Lett.*, vol. 39, no. 10, pp. 800–803, 1981.

[22] S. Kang *et al.*, "Detailed analysis and performance limiting mechanism of Si delta-doped GaAs tunnel diode grown by MBE," *Jpn. J. Appl. Phys.*, vol. 57, no. 12, 2018, Art. no. 120306.

[23] G. C. DeSalvo, "Ultrathin delta doped GaAs and AlAs tunnel junctions as interdevice ohmic contacts," *J. Appl. Phys.*, vol. 74, no. 6, pp. 4207–4212, 1993.

[24] F. W. Ragay, E. W. M. Ruigrok, and J. H. Wolter, "GaAs-AlGaAs heterojunction solar cells with increased open-circuit voltage," in *Proc. IEEE 1st World Conf. Photovoltaic Energy Convers.*, 1994, pp. 1934–1937, doi: 10.1109/WCPEC.1994.520747.

[25] J. K. Kung and W. G. Spitzer, "Effects of annealing on the carrier concentration of heavily Si-doped GaAs," *J. Appl. Phys.*, vol. 44, no. 2, pp. 912–914, 1973.

[26] Y. Sun *et al.*, "Delta-doping for enhanced tunnel junction performance and thermal stability," in *Proc. IEEE 46th Photovolt. Specialists Conf.*, 2019, pp. 3211–3214, doi: 10.1109/PVSC40753.2019.8980681.

[27] D. J. Friedman, A. E. Kibbler, and R. Reedy, "Selection of substrate orientation and phosphorus flux to achieve p-type carbon doping of Ga0.5In0.5P by molecular beam epitaxy," *Appl. Phys. Lett.*, vol. 71, no. 8, pp. 1095–1097, 1997.

[28] H. Aldridge *et al.*, "N-type doping strategies for InGaAs," *Mater. Sci. Semicond. Process.*, vol. 62, pp. 171–179, 2017.

[29] T. Masuda, S. Tomasulo, J. R. Lang, and M. L. Lee, "Comparison of single junction AlGaInP and GaInP solar cells grown by molecular beam epitaxy," *J. Appl. Phys.*, vol. 117, no. 9, 2015, Art. no. 094504.

[30] K. L. Schulte *et al.*, "Growth of AlGaAs, AlInP, and AlGaInP by hydride vapor phase epitaxy," *ACS Appl. Energy Mater.*, vol. 2, no. 12, pp. 8405–8410, 2019.

[31] K. L. Schulte *et al.*, "Development of GaInP solar cells grown by hydride vapor phase epitaxy," *IEEE J. Photovolt.*, vol. 7, no. 4, pp. 1153–1158, Jul. 2017.

[32] E. E. Perl *et al.*, "Development of high-bandgap AlGaInP solar cells grown by organometallic vapor-phase epitaxy," *IEEE J. Photovolt.*, vol. 6, no. 3, pp. 770–776, May 2016, doi: 10.1109/JPHOTOV.2016.2537543.

[33] H. Sodabanlu *et al.*, "High-Speed MOVPE growth of InGaP solar cells," *IEEE J. Photovolt.*, vol. 10, no. 2, pp. 480–486, Mar. 2020, doi: 10.1109/JPHOTOV.2020.2964994.

[34] D. Meyerhofer, G. A. Brown, and H. S. Sommers, "Degenerate germanium. I. Tunnel, excess, and thermal current in tunnel diodes," *Phys. Rev.*, vol. 126, no. 4, pp. 1329–1341, 1962.

[35] E. Barrigón, I. García, L. Barrutia, I. Rey-Stolle, and C. Algora, "Highly conductive p^{++}-AlGaAs/n^{++}-GaInP tunnel junctions for ultra-high concentrator solar cells," *Prog. Photovolt. Res. Appl.*, vol. 22, no. 4, pp. 399–404, 2014.

[36] I. Rey-Stolle *et al.*, "On the thermal degradation of tunnel diodes in multijunction solar cells," *AIP Conf. Proc.*, vol. 1881, no. 1, Sep. 2017, Art. no. 040005.